Lattice dynamics and molecular-dynamics study of quartz using a many-body variable potential

Y. Ma and S. H. Garofalini
Interfacial Molecular Science Laboratory, Department of Materials Science and Engineering, Rutgers University, Piscataway, New Jersey 08854, USA
(Received 17 February 2006; published 10 May 2006)

A many-body variable potential is used to study the structural phase transition of quartz. The most significant feature of this variable potential is that the parameters are separately fitted to two phases of quartz and are allowed to change as a function of temperature to account for any nuclear and electronic excitations at finite temperature. Lattice dynamics calculations at room temperature showed that this variable potential describes the dynamical properties of α-quartz with good accuracy. Molecular-dynamics calculations at various temperatures showed that the structural phase transition of quartz, as well as the associated anomalies, is well described by this variable potential. Analysis of the β phase at high temperature favored a disordered picture of the structure.

DOI: 10.1103/PhysRevB.73.174109 PACS number(s): 71.15.Pd, 81.30.−t, 34.20.Cf

I. INTRODUCTION

Although intensive efforts, both experimentally and theoretically, have been made toward the understanding of the structural phase transition in quartz, the microscopic mechanism has yet to be clarified. The room temperature phase of quartz, or α-quartz, has trigonal symmetry described by space group $P3_121$. At 847 K, it undergoes a structural transition and transforms into the high-temperature β phase with space group $P6_222$, accompanied by abrupt changes in thermal expansion, elastic moduli, etc. A number of x-ray and neutron diffraction, as well as NMR studies have been carried out to investigate accurately the detailed structural evolution involved in the α-β transition.[1–3] Elastic constants at various temperatures have also been determined by different authors.[4,5]

The nature of the structure of the β phase, unfortunately, remains a controversial problem. It is well established that there exist two potential minima in the α phase, α_1 and α_2, corresponding to Dauphine twinning. The structure of the two equivalent phases can be characterized by the position of silicon and oxygen atoms, whose fractional coordinates in the α_1 and α_2 phase are $[\mathrm{Si}(u,0,0),\mathrm{O}(x,y,z)]$ and $[\mathrm{Si}(1-u,0,0),\mathrm{O}(x,x-y,1/3-z)]$, respectively. In the β phase, however, whether the α_1 and α_2 survive or not is still unclear. Experimentally the actual structure of the β phase is very difficult to characterize due to the microscopic nature of the problem. Theoretically, molecular modeling would be an ideal tool to investigate this issue.

To draw an unambiguous microscopic picture, a relatively large number of atoms have to be included in the modeling, which is obviously computationally very expensive for any first-principles method. Molecular-dynamics (MD) simulations, however, do not suffer from such a limitation; more atoms can be simulated and the time scale on which any statistical sampling can be taken can be much longer. Thus MD simulation is particularly suitable for the study of the change in the microstructure as well as macroscopic properties associated with a phase transition.

The quality of any MD simulation is determined by the interatomic potential used in the simulation. For the study of quartz, a number of empirical potentials exist in the literature.[6–9] Among them, the Tsuneyuki-Tsukada-Aoki-Matsui (TTAM) and Beest-Kramer-Santen (BKS) pair potentials were initially fitted from *ab initio* calculations and have been widely used to study silica polymorphs.[10–15] It is generally observed that both TTAM and BKS potentials are able to describe the silica polymorphs with reasonable accuracy, although the BKS potential is in slightly better agreement with experiments. This is because the *ab initio* parametrization was modified to better coincide with experimental data. Most of the MD studies favored the disordered structure of the β phase,[10,11] although dispute still exists.[14] Lattice-dynamics (LD) studies derived from the TTAM potential have also been carried out,[16,17] in which the ideal β structure is found to be incompatible with observed elastic properties[16] and the author concluded that the β structure is essentially dynamical.[17]

Despite the success of the TTAM and BKS potentials, their limitations are obvious. First, although fractional charges are used in both of the two potentials to account for the fact that quartz is largely a covalent material, it is assumed that all the charges are pointlike. However, the point-charge assumption is known to be problematic, especially for short interatomic distances.[18–20] Second, any possible effects on the nuclear dynamics due to the change of the electronic structure with temperature are being omitted. Of course, an accurate determination of electronic structure is certainly beyond the scope of classical simulations. However, semi-empirical methods do exist.[19,21] In fact, both potentials are far from perfect. The calculated equilibrium unit cell volume is about 7% larger than the experimental results.[10] The equilibrium Si-O-Si angle is also overestimated,[13] which might be a result of the lack of three-body potential necessary for the description of the directional bond in quartz.

In this paper, we present the results of lattice dynamics and molecular-dynamics calculations on the α-β phase transition in quartz using a many-body empirical potential. This potential has been successfully applied to the study of thermal, mechanical, and elastic properties of bulk SiC.[22] The non-point-charge effect has been taken into account explicitly in an empirical manner. The long-range Coulomb term is

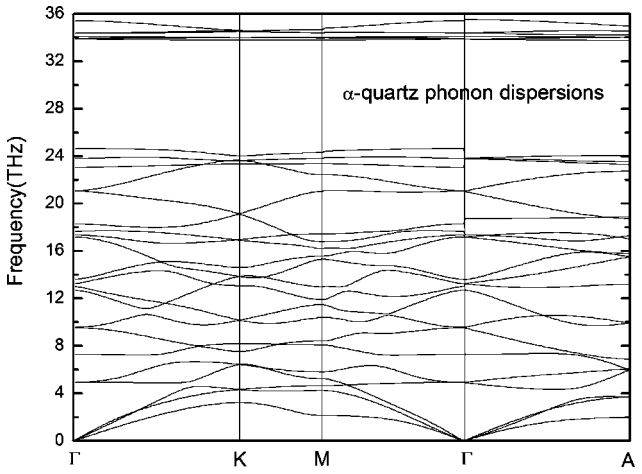

FIG. 1. Phonon dispersion curves for α-quartz at 293 K based on experimentally determined structure (Ref. 2). For a direct comparison with experimental phonon frequencies, see Table V. Note that 36 THz corresponds to 1200 cm^{-1}, approximately.

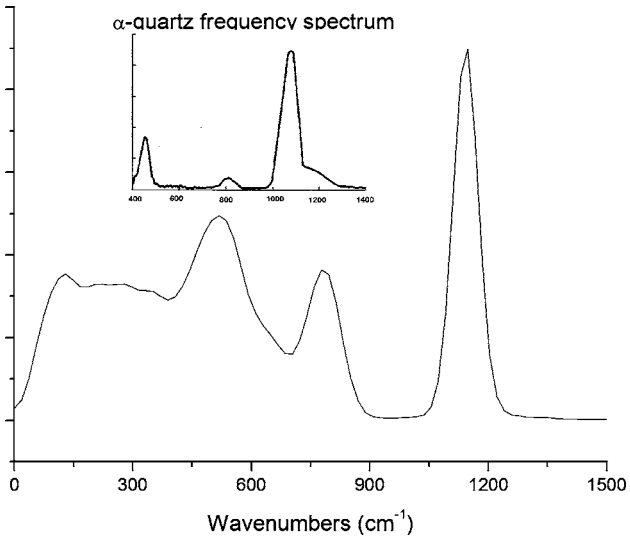

FIG. 2. Frequency spectrum calculated by MD at 293 K. Inset: experimental spectrum from Ref. 44.

evaluated using a modified Wolf sum approach.[23,24] An important feature of this potential is that the parameters are allowed to vary as a function of system temperature, which essentially means that the system is able to evolve on a set of adiabatic Born-Oppenheimer surfaces. In most MD studies, a single potential energy surface (PES) is used in the consideration that any electronic variations are unimportant. However, it is clear that there must be some alteration in the electronic structure to effect a change in the atomistic structure of different phases. This is evidenced by the application of variable charge potentials,[19,20,25] which, however, only change the charges and not necessarily other parameters in the potential. In fact, our results show that by introducing the variable PES, the accuracy of the simulated quartz structure improves significantly. Interest in other forms of environment-dependent potentials is growing, although these potentials can become extremely complicated.[26–28] Of course a perfect match with experimental data may not be possible, although better accuracy offers more reliable predictions from simulations.

This paper is organized as follows. In Sec. II, the detailed computational methods used in this study will be discussed. The results of our LD and MD calculations will be presented in Sec. III. A conclusion section then follows.

II. COMPUTATIONAL METHODS

A. Potential energy function

The details of the potential energy function has been given elsewhere.[24] In short, it includes a modified Wolf sum term, a Morse-stretch term, and a three-body term:

$$E^{\mathrm{Wolf}} = \frac{1}{2}\sum_i \sum_{\substack{j\neq i \\ r_{ij}\leqslant R_c}} \left(\frac{q_i q_j}{r_{eff}} - \frac{q_i q_j}{r_{ij}}\right) + \frac{1}{2}\sum_{i=1}^{N} \sum_{\substack{j\neq i \\ r_{ij}<R_c}} \left[\frac{q_i q_j \,\mathrm{erfc}(r_{ij}/\beta)}{r_{ij}} - \lim_{r_{ij}\to R_c}\left(\frac{q_i q_j \,\mathrm{erfc}(r_{ij}/\beta)}{r_{ij}}\right)\right] - \left(\frac{\mathrm{erfc}(R_c/\beta)}{2R_c} + \frac{1}{\beta\pi^{1/2}}\right)\sum_{i=1}^{N} q_i^2, \tag{1a}$$

$$E^{M\text{-}S} = \frac{1}{2}\sum_i \sum_{\substack{j\neq i \\ r_{ij}<R_c}} D_0\{\exp[K_0(1-r_{ij}/R_0)] - 2\exp[K_0/2(1-r_{ij}/R_0)]\}, \tag{1b}$$

$$E^{(3)}(r_{ij}, r_{ik}, r_{jk}) = \left[\lambda_{jik}\exp\left(\frac{\gamma_{ij}}{r_{ij}-r_{ij}^c} + \frac{\gamma_{ik}}{r_{ik}-r_{ik}^c}\right) \times \left(\cos\theta_{jik} + \frac{1}{3}\right)^2\right]. \tag{1c}$$

r_{eff} is defined as

TABLE I. Parameters for electrostatic interactions.

q_{Si}	q_{O}	R_c (10^{-8} cm)	β (10^{-8} cm)	$\zeta_{\mathrm{Si\text{-}Si}}$ (10^8 cm^{-1})	$\zeta_{\mathrm{Si\text{-}O}}$ (10^8 cm^{-1})	$\zeta_{\mathrm{O\text{-}O}}$ (10^8 cm^{-1})
1.6	−0.8	10	3.8	4.2236	4.9193	5.7295

$$r_{eff} = \left(r^3 + \frac{\mathrm{erfc}\left(\frac{r-r'}{r''}\right)}{2} \frac{1}{\zeta_{ij}^3} \right)^{1/3}. \quad (2)$$

In Eq. (1a), the last two terms are exactly the same as in the original Wolf sum,[23] where q_i and q_j are charges on the atoms, β is the damping parameter, and R_c is the cutoff distance. The first term in Eq. (1a) is introduced to account for the non-point-charge effects, especially at short interatomic distances. r_{eff}, defined in Eq. (2), is an empirical evaluation of the Coulomb integral between two charge densities.[18] Note that a complementary error function has been added in r_{eff} such that by appropriate choices of r' and r'', r_{eff} and all its higher derivatives approach continuously to r at R_c, thus avoiding any discontinuity at the cutoff distance. The Morse-stretch energy function has also been added to account for the covalent interactions. To describe the directional bonds in quartz, a three-body term is used where i is the central atom with nearest neighbors j and k, and θ_{jik} is the angle between r_{ij} and r_{ik} with the vertex at i. All the parameters in Eqs. (1) and (2) are given in Tables I–IV.

B. Calculation of elastic constants and phonon frequencies

Under the harmonic approximation, the phonon frequencies, elastic constants, etc, can be derived from any empirical force field by taking appropriate second derivatives and forming the dynamical matrix with matrix elements defined as[29–31]

$$D_{\alpha\beta}(kk'|K) = (m_k m_{k'})^{1/2} \sum_{l'} \Phi_{\alpha\beta}(lk;l'k') \times \exp\{-iK[X(lk) - X(l'k')]\} \quad (3)$$

$\Phi_{\alpha\beta}(lk;l'k')$ is known as the atomic force constant. Diagonalization of the dynamical matrix gives the square of phonon frequencies at any K point compatible with boundary conditions.

The elastic constants are evaluated by[29–31]

$$C_{\alpha\gamma\beta\lambda} = [\alpha\beta,\gamma\lambda] + [\gamma\beta,\alpha\lambda] - [\alpha\gamma,\beta\lambda] + (\alpha\gamma,\beta\lambda) \quad (4a)$$

with

$$[\alpha\beta,\gamma\lambda] = \frac{1}{2V_0} \sum_{kk'} (m_k m_{k'})^{1/2} C^{(2)}_{\alpha\beta,\gamma\lambda}(kk'), \quad (4b)$$

TABLE II. Parameters for three-body interactions.

	r_i^c (10^{-8} cm)	λ (10^{-11} ergs)	γ (10^{-8} cm)
O-Si-O	2.6	0.2904	2.0
Si-O-Si	3.0	9.714	2.6

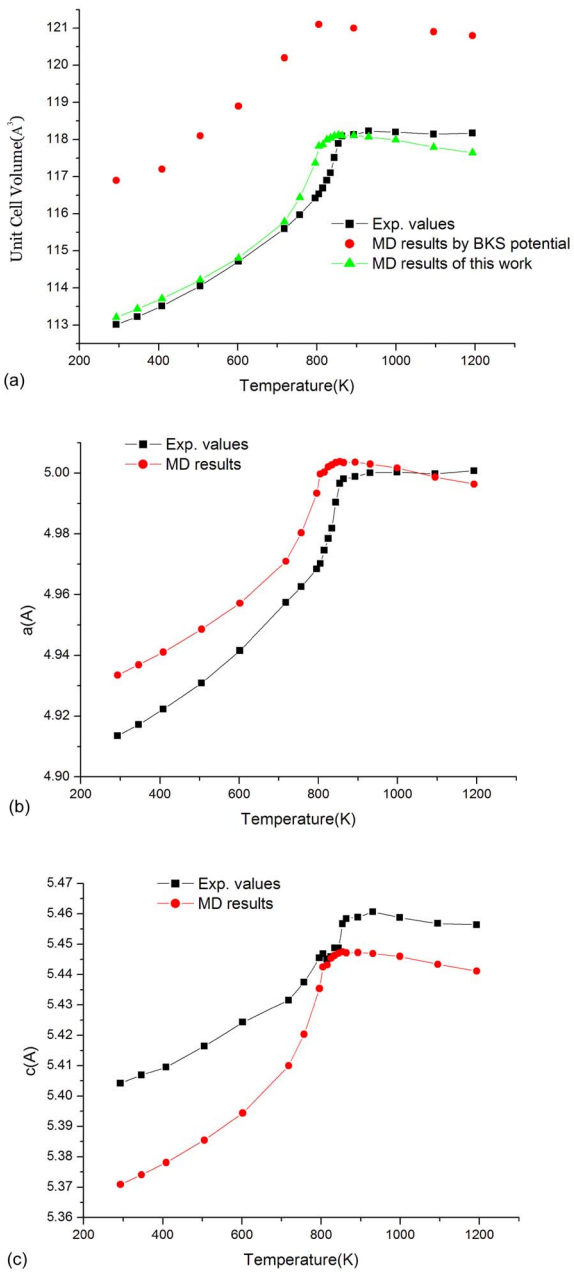

FIG. 3. (Color online) Thermal expansion of quartz from 293 to 1193 K. Experimental values are from Ref. 2. The BKS results are adapted from Ref. 14. (a) Equilibrium volume; (b) lattice constant a; (c) lattice constant c.

$$(\alpha\gamma,\beta\lambda) = -\frac{1}{V_0} \sum_{kk'} \sum_{\mu\nu} \Gamma_{\mu\nu}(kk') \left(\sum_{k''} (m_{k''})^{1/2} C^{(1)}_{\mu\alpha,\gamma}(kk'') \right) \times \left(\sum_{k'''} (m_{k'''})^{1/2} C^{(1)}_{\nu\beta,\lambda}(k'k''') \right). \quad (4c)$$

Here $C^{(1)}$ and $C^{(2)}$ are the first and second derivatives of the dynamical matrix D, and Γ is the inverse of D, with the three acoustic modes removed. V_0 is the volume of the primitive cell, and m_k is the mass of atom k.

As long as the anharmonic effects are negligible, the above calculations can be performed straightforwardly to obtain for an infinite crystal lattice the elastic constants and phonon dispersion relations. The anharmonic effects are closely related to the magnitude of atomic vibrations around their equilibrium positions. Thus, one would expect that the LD calculations within the harmonic approximation would fail at high T. MD simulation, on the other hand, includes any anharmonic effects in an exact manner. In this paper, the elastic constants at various temperatures are evaluated by the so-called fluctuation formula[32,33]

$$C_{\alpha\gamma\beta\lambda} = -\frac{V}{k_B T}\delta(P_{\alpha\gamma}P_{\beta\lambda}) + \frac{2Nk_B T}{V}(\delta_{\alpha\lambda}\delta_{\gamma\beta} + \delta_{\alpha\beta}\delta_{\gamma\lambda}) + \frac{1}{V}\left\langle \sum_{b>a} f(r_{ab}) x_{ab\alpha} x_{ab\gamma} x_{ab\beta} x_{ab\lambda} \right\rangle_{av}, \quad (5)$$

where $P_{\alpha\gamma}$ is the internal stress tensor, and V is the volume of the simulation cell containing N atoms. The first, second, and third terms in Eq. (5) are referred to as the fluctuation, kinetic, and Born terms, respectively. Note that the three-body contribution has to be included in both the internal stress tensor $P_{\alpha\gamma}$ and the potential energy derivatives $f(r)$.

To ensure that the calculated elastic constants correspond to zero stress, a constant-pressure, constant-temperature (NPT) simulation is carried out using the Nosé-Hoover-Parrinello-Rahman algorithm.[34–36] The equation of motion is integrated using an explicit reversible integrator[37] with a time step of 1 fs. Initially, the atoms are put on the experimental positions at 293 K (Ref. 2) and assigned velocities corresponding to a Gaussian distribution around the system temperature of 293 K. Then the temperature of the system is raised at the rate of 25 K/ps to the desired temperature. An equilibration period of 100 ps at temperature occurs before the statistical averages are taken. After constructing the reference structure of zero stress at each temperature, the fluctuation formula is then used to obtain the adiabatic elastic constants. Due to the poor convergence of the fluctuation term, the elastic constants are averaged over 1.5 ns. All of the MD calculations are performed for a system containing 1080 ($5\times6\times4$ α-quartz unit cells) atoms. The temperature range studied is from 293 to 1193 K.

C. Parametrization using a genetic algorithm

The parameters used in this work are optimized to reproduce accurately the lattice constants and elastic moduli across the phase transition. As discussed above, the parameters are allowed to change as a function of T, which gives the potential great flexibility in describing the structural and elastic properties. However, such functional dependence is not known *a priori* and can only be determined empirically. Intuitively, one can determine for each temperature under study an optimal set of parameters and then work out the functional dependence. To simplify, however, only the parameters at 293 K, corresponding to the low-temperature α phase, and at 893 K, corresponding to the high-temperature β-phase, are first determined. All the other parameters at each T are just linearly interpolated. Surprisingly, this simple linear interpolation works reasonably well, although multiple phases and temperature regimes might allow for a more complicated, and possibly more accurate, interpolation formula.

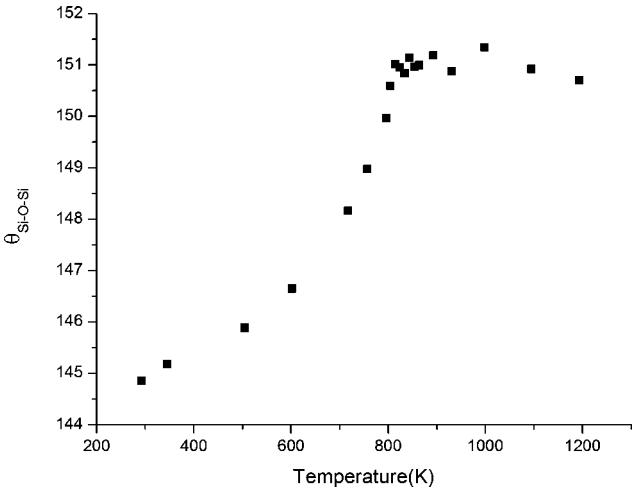

FIG. 4. Evolution of Si-O-Si bond angle with temperature.

As given in Eqs. (1a)–(1c), the potential contains contributions from electrostatic, Morse-stretch, and three-body interactions. Thus, a complete "variable parameters" scheme would require that all of the parameters used in the above interactions are temperature variable. For the electrostatic interaction, this can be done by introducing a "variable charge" method such as charge equilibration (Qeq) or electronegativity equalization method (EEM).[19,21] However, both of these two methods involve solving a large sparse matrix at each nuclear iteration and are computationally expensive. Indeed, the calculated semiempirical charges in the α and β phases of quartz differ little[38] due to the close resemblance of the two structures. Moreover, although the local charge distribution may differ significantly, the bulk properties will not depend on local deviations on an average sense. Base on the above arguments, we currently keep the charge distribution fixed in all of the simulations, as given in Table I. Keep in mind, however, that a variable charge scheme would be advantageous when dealing with surfaces or interfaces.

TABLE III. Parameters for the Morse-stretch potential at 293 K.

	D_0 (10^{-12} ergs)	K_0	R_0 (10^{-8} cm)
Si-Si	0.045582	10.264	4.3656
Si-O	6.9622	7.4251	1.5236
O-O	0.027668	10.301	4.008

TABLE IV. Parameters for Morse-stretch potential at 893 K.

	D_0 (10^{-12} ergs)	K_0	R_0 (10^{-8} cm)
Si-Si	0.044674	10.045	4.4380
Si-O	6.5873	7.4604	1.5237
O-O	0.026416	10.084	4.002

The three-body parameters are also kept fixed considering that the three-body terms contribute less than 1% of the total energy. All of the parameters used in the three-body interaction are listed in Table II.

Finally, the parameters in the Morse-stretch potential energy are able to vary as a linear function of T. A genetic algorithm is used for parameter optimization. At 293 K, the fitness function used is given as

$$f = -(p-p_0)^2 - \sum_{i,j}(C_{ij}-C_{ij}^0)^2 - \sum_{i,K}(\omega_{i,K}-\omega_{i,K}^0)^2 \quad (6)$$

where p is the calculated internal pressure, C_{ij} are the elastic constants in Voigt notation, and $\omega_{i,K}$ denotes the ith phonon frequency at point K in the first Brillouin zone. The superscript 0 denotes the respective experimental values, while p_0 was set to zero corresponding to the zero-stress condition. The LD calculation based on the experimental structure at 293 K is used to obtain C_{ij} and $\omega_{i,K}$. It is not possible to calculate all the phonon frequencies and in practice only a few frequencies at high-symmetry points are included. Also note that there is an underlying assumption when performing LD calculations: the anharmonic effects are negligible. The validity of this assumption is proved by our MD results, as will be shown in the next section.

The genetic algorithm is then able to maximize the fitness function given in Eq. (6). The parameters that give the maximal fitness value are then the desired parameters at 293 K, as listed in Table III.

At 893 K, the LD calculations are no longer valid. Only the first term in Eq. (6) is kept as the fitness function at 893 K. At the same time, the parameter search space is greatly reduced to be within ±5% of the fitted parameters at 293 K based on the consideration that the change in the PES is moderate. All the parameters at 893 K are listed in Table IV. Parameters at other temperatures are linearly interpolated.

III. RESULTS AND DISCUSSION

A. Vibrational normal modes

In the fitting of parameters at 293 K, only a few phonon frequencies at high-symmetry points are used in the fitness function. Using the fitted parameters, the whole phonon spectrum is then calculated as shown in Fig. 1. The results are in good agreement with experiments as well as earlier theoretical works.[30,39–41] For a direct comparison with experiment, Table V lists some of the calculated phonon frequencies along with the experimental data.[39–41] For frequencies at the zone center, the calculated root mean square difference is 60 cm^{-1}, slightly better than those reported for the TTAM potential [76 cm^{-1} (Ref. 42)] and the BKS potential [68 cm^{-1} (Ref. 13)]. Interestingly, all three potentials overestimated the low-energy phonons whereas high-energy phonons are underestimated, which can be related to the approximate nature of the empirical force fields.

In MD calculations, the vibrational frequency spectrum can be generated by the Fourier transformation of the velocity autocorrelation function.[43] As a comparison with the above LD results, MD calculation of the frequency spectrum at 293 K is then carried out and the result is plotted in Fig. 2. The experimental infrared absorption spectrum is also given.[44] The agreement is also satisfactory, with all of the major peaks reproduced.

TABLE V. Calculated and experimental phonon frequencies (Refs. 39–41). The experimental data are measured at room temperature, while the calculation is performed at 293 K. Comparison with the results by the TTAM potential (Ref. 42) is made when available.

		Phonon frequencies (cm^{-1})		
K point	Symmetry	This work	TTAM	Experiment
$\Gamma(0,0,0)$	A_1	243	243	207
		424	403	356
		580	541	464
		1137	980	1085
	A_2	435	437	364
		591	622	495
		767	696	778
		1131	1007	1080
	E_T	164	163	128
		319	301	265
		443	426	394
		574	580	450
		702	663	697
		795	706	795
		1129	990	1072
		1147	1110	1162
	E_L	164	163	128
		319	301	265
		455	440	401
		611	637	509
		704	675	697
		823	779	807
		1147	1094	1162
		1181	1134	1235
$A(0,0,1/2c)$	A_2	65		52
	E	122		119
	E	199		170
	A_2	201		195
	A_1	230		200
	E	332		268
$M(1/a,0,0)$	T_2	71		70
	T_2	141		120
	T_1	154		143
	T_2	174		144
	T_1	193		180
	T_1	270		237

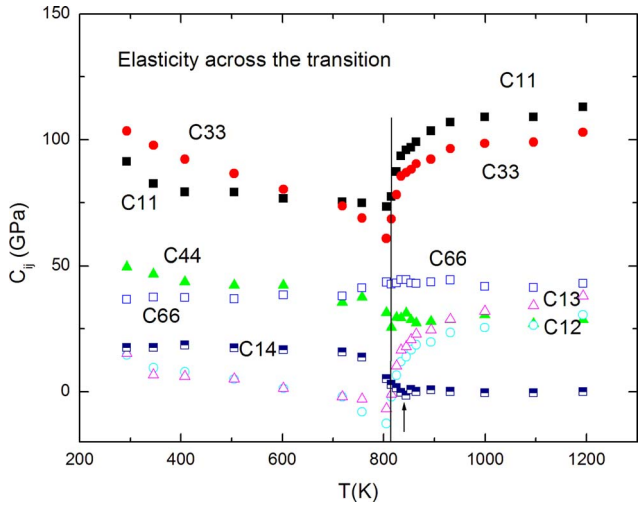

FIG. 5. (Color online) Evolution of the elastic constants with T. The vertical line indicates the start of the structural phase transition. The arrow indicates the point where C_{14} vanishes, as required by β-quartz symmetry. Filled square, C_{11}; filled circle, C_{33}; filled triangle, C_{44}; open square, C_{66}; open circle, C_{12}; open triangle, C_{13}; half-filled square, C_{14}.

B. Thermal expansion across the transition

From 293 to 1193 K, the lattice parameters of quartz have been determined by the Parrinello-Rahman method and the temperature of the system was controlled by a Nosé-Hoover thermostat.[34–36] Along with experimental results,[1] the calculated equilibrium volume and lattice constants are plotted in Fig. 3. The results obtained by the BKS potential are also shown. The calculated equilibrium volumes are within 1% of the experimental value for the whole temperature regime, which is a substantial improvement over both the BKS and TTAM potentials. The errors in lattice constants a and c are also within 1%. The correct anomaly in thermal expansion is reproduced with good accuracy. The predicted transition is around 840 K, which is in close agreement with the experimentally determined value 847 K. Figure 4 shows the calculated Si-O-Si bond angle, in which the transition from the α phase, where the bond angle assumes an average value of 144°, to the β phase, where the bond angle is around 151°, is clearly seen. The only failure of this potential is the ability to predict the anomaly in the c/a ratio. The calculated c/a ratio decreases slightly with increasing T and no abrupt change has been observed. Similar results are reported for the BKS and TTAM potentials, where the authors argue that lack of a three-body term may be responsible for the failure in describing the c/a ratio.[14] Such an argument, however, cannot be verified in our study. The origin of the c/a anomaly is yet to be determined.

Although in the temperature range studied in this work, all of the lattice parameters are in good agreement with experiments, one should notice that starting from 1000 K the error in calculated lattice parameters increases. Considering that only a linear function has been used to determine the variable parameters, and only the Morse terms are varied, such an increase in error with temperature suggests the use of a more complicated function based on the additional high-temperature phase cristobalite, which would give more flexibility in accurately reproducing all of the experimental data. However, the advantage of using a variable potential based on a simple interpolation between phases is clear.

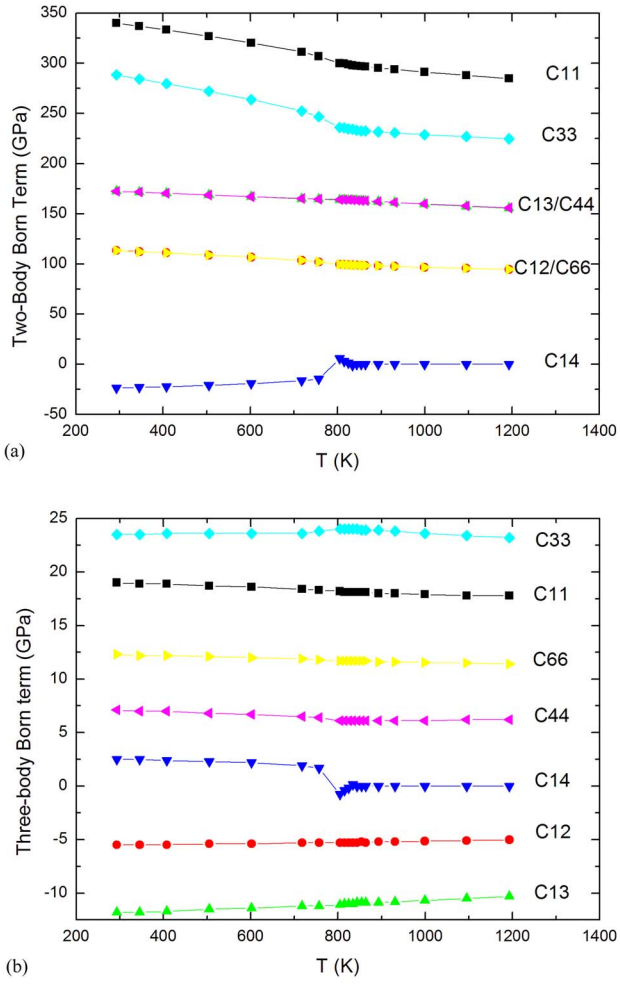

FIG. 6. (Color online) Comparison of (a) two-body and (b) three-body Born term.

C. Elasticity across the transition

Based on the calculated equilibrium zero stress structure at each T, the elastic constants are calculated and plotted in Fig. 5. Table VI gives the calculated and experimental values at 293 and 893 K.[4,5] At 293 K, both LD and MD results are shown. It is interesting to note that although the 293 K parameters are fitted by LD data, the MD calculated results using the fluctuation formula do not differ significantly. All the differences can thus be traced back to any possible anharmonic effects, which obviously do not play any important role at 293 K.

By a careful examination of the elasticity across the transition, as shown in Fig. 5, we assert that our potential model gives a satisfactory description of the elastic anomalies found in quartz. Due to the poor convergence of the fluctuation term in the fluctuation formula, as well as the finite-size effect, our calculated results may be subject to statistical un-

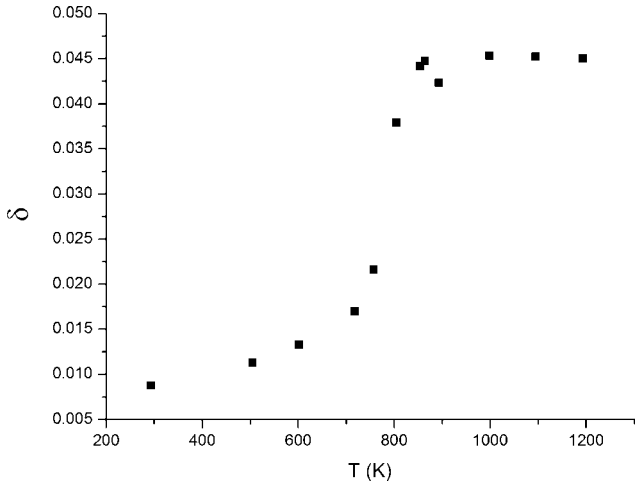

FIG. 7. Temperature dependence of order parameter δ, averaged over the simulation cell and over 10 ps.

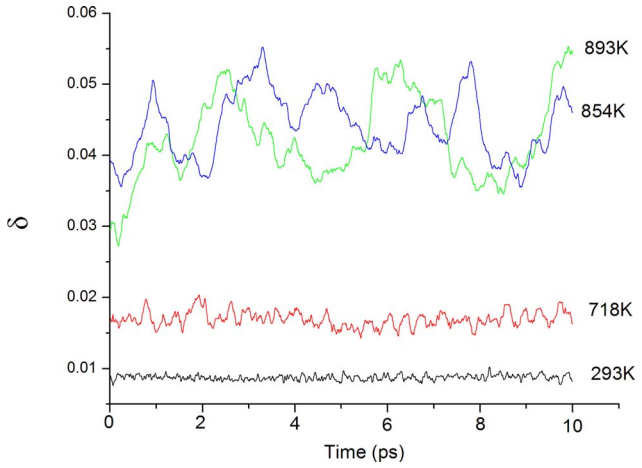

FIG. 8. (Color online) Time evolution of δ, averaged over the simulation cell.

certainty. However, the obvious change in elasticity around the transition point clearly suggests the place of the structural phase transition. In particular, the calculated dependence of elastic constants on T is in reasonably good agreement with experiment.[1] The abrupt change in elasticity starts at around 820 K, as indicated by the vertical line in Fig. 5. However, at this point, the phase transition is not yet complete, as C_{14} remains a non-negligible value. The vanishing of C_{14} occurs around 840 K, which suggests that the symmetry of the structure has changed from trigonal to hexagonal at this point.

Unlike from both the BKS and TTAM potentials, the potential used in this study includes a three-body term. Thus, it is interesting to examine the contribution of the three-body potential to the elastic constants as compared to the two-body energy. In Fig. 6, the two-body and three-body Born terms are plotted against T. Clearly, the three-body term is an order of magnitude smaller than the two-body term, which explains partly why the two-body potentials in the literature also reasonably reproduce the elasticity of quartz. However, although small, the three-body contributions are clearly non-negligible. Even though their contribution to the total energy is less than 1%, their contribution to the elastic constants could be as high as 10%.

TABLE VI. Adiabatic elastic constants at 293 K (Ref. 4) and 893 K (Ref. 5). The experimental values are from Ref. 3.

	α-quartz (293 K)			β-quartz (893 K)	
	LD	MD	Expt.	MD	Expt.
C_{11}	88.2	91.4	86.7	103.5	118.4
C_{12}	5.9	14.5	7.0	19.7	19.0
C_{13}	7.7	15.2	11.9	24.5	32.0
C_{14}	12.4	17.5	17.9	0.7	
C_{33}	103.9	103.5	107.2	92.3	107.0
C_{44}	58.6	49.6	57.9	27.9	35.8
C_{66}	41.1	36.7	39.8	43.6	49.7

Another feature of the calculated Born terms is that almost no sudden changes are observed at the transition T, except for C_{14}. Thus, it can be concluded that the elastic anomalies are mainly the results of the internal stress relaxation which contributes to the fluctuation term.

D. Dauphine twinning and the β-quartz structure

According to Tsuneyuki *et al.*,[10] $u-1/2$ can be chosen as the order parameter of the phase transition, where u is the atomic coordinate of the Si atom. For an ideal β structure, $u-1/2$ should be zero. An order parameter defined in this way can certainly give some indications of the structural change. However, the contribution from the oxygen atoms in the primitive cell is missing. In this work, we define the order parameter to be the root mean square displacement of each atom in the primitive cell from their equilibrium position in α_1 phase:

$$\delta = \sqrt{[(u-u_0)^2 + (x-x_0)^2 + (y-y_0)^2 + (z-z_0)^2]/4} \quad (7)$$

where u_0, x_0, y_0, z_0 are the experimentally determined positions[2] corresponding to the α_1 structure. It is straightforward to show that the value for δ is 0.084 for the α_2 phase, while it is 0 for α_1. Thus by tracking the evolution of δ, one can gain qualitative insight into the nature of the structure.

Figure 7 plots the average of δ over the simulation cell and over a time frame of 10 ps from 293 to 1193 K. The evolution from the α_1 to the β phase is clearly seen. However, the microscopic feature of the β phase should not be disguised by the time-averaged δ value. For this purpose, the time evolutions of δ at 293 and 718 K, corresponding to the α structure, and 854 and 893 K, corresponding to the β phase, are plotted in Fig. 8. The averages are taken over all of the primitive cells in the simulation cell and are recorded for 10 ps. The behavior of δ at 293 and 718 K is due to the thermal motions of the atoms in the α phase. At 854 and 893 K, however, different domains clearly exist. The same kind of behavior has been reported for the order parameter $u-1/2$, where the correlation length and time are greatly reduced at 900 K.[10] In this study, no obvious change has

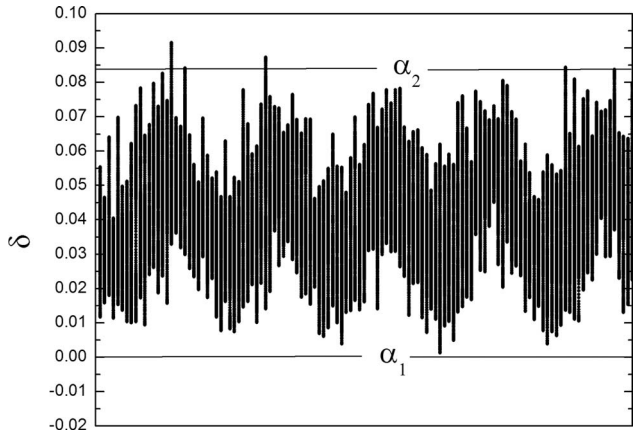

FIG. 9. The cumulative distribution of δ in the simulation cell. The solid line corresponds to the α_1 and α_2 phases.

been observed for the correlation length and time at the temperature of 893 K. The existence of α_1 and α_2 domains in the β phase is further proved by the distribution of δ in the simulation cell, as shown in Fig. 9. Even though a relatively small simulation cell has been used in this study ($5\times6\times4$), it is clear from Fig. 9 that different domains exist. Thus, our study has provided additional evidence for the disordered structure of the β phase.

IV. CONCLUSION

In this work, a many-body variable potential has been used to study the structural phase transition in quartz. The main feature of this study is that some of the parameters are designed to be accurate for individual phases and are allowed to vary as a function of an external variable (here, temperature) to give more flexibility for the potential in describing macroscopic properties. The calculated results on quartz from 293 to 1193 K show that this potential is able to describe the α-β phase transition and the associated anomalies with better accuracy than the more popular TTAM or BKS potentials. Moreover, attempts to clarify the microscopic nature of the β phase reached the conclusion that the β phase is essentially dynamical and is realized by the average of the α_1 and α_2 phases.

The closer agreement with the experimental data shown in this work indicates the benefit of even this very simple two phase linear interpolation of the variable parameters based on accurate results for individual phases. Our work thus suggests a simple way to achieve such transferability with improved accuracy in materials modeling, regardless of the form of the potentials. It can also be extended to allow for even larger flexibility by including variable charges, more phases and pressure, temperature, or volume-dependent parameters that can be used in the simulations of materials under various conditions. The validity of this variable parameter approach can be checked by a direct comparison with the high-quality experimental data.

ACKNOWLEDGMENTS

The authors acknowledge support from the U.S. Department of Energy, Office of Science, Basic Energy Sciences, Division of Chemical Sciences, Geosciences, and Biosciences, Grant No. DE-FG02-93ER14385. Y.M. also acknowledges partial support from NSF, Grant No. DMR-0010062, in collaboration with the NANOAM project of EU-CORDIS (Grant No. G5RD-CT-2001-00586).

[1] M. A. Carpenter *et al.*, Am. Mineral. **83**, 2 (1998).
[2] A. F. Wright and M. S. Lehmann, J. Solid State Chem. **36**, 372 (1981).
[3] D. R. Spearing, I. Farnan, and J. F. Stebbins, Phys. Chem. Miner. **19**, 307 (1992).
[4] R. Bechmann, Phys. Rev. **110**, 1060 (1958).
[5] E. W. Kammer and J. V. Atanasoff, Phys. Rev. **62**, 395 (1942).
[6] B. P. Feuston and S. H. Garofalini, J. Chem. Phys. **89**, 5818 (1988).
[7] J. Sefcik *et al.*, J. Comput. Chem. **23**, 1507 (2002).
[8] S. Tsuneyuki, M. Tsukada, H. Aoki, and Y. Matsui, Phys. Rev. Lett. **61**, 869 (1988).
[9] B. W. H. van Beest, G. J. Kramer, and R. A. van Santen, Phys. Rev. Lett. **64**, 1955 (1990).
[10] S. Tsuneyuki, H. Aoki, M. Tsukada, and Y. Matsui, Phys. Rev. Lett. **64**, 776 (1990).
[11] H. Kimizuka, H. Kaburaki, and Y. Kogure, Phys. Rev. B **67**, 024105 (2003).
[12] R. Guido, D. Valle, and H. C. Andersen, J. Chem. Phys. **94**, 5056 (1990).
[13] J. S. Tse and D. D. Klug, J. Chem. Phys. **95**, 9176 (1991).
[14] M. H. Muser and K. Binder, Phys. Chem. Miner. **28**, 746 (2001).
[15] H. Kimizuka and H. Kaburaki, Phys. Status Solidi B **242**, 607 (2005).
[16] M. B. Smirnov and A. P. Mirgorodsky, Phys. Rev. Lett. **78**, 2413 (1997).
[17] M. B. Smirnov, Phys. Rev. B **59**, 4036 (1999).
[18] J. N. Louwen and E. T. C. Vogt, J. Mol. Catal. A: Chem. **134**, 63 (1998).
[19] A. K. Rappe and W. A. Goddard, J. Phys. Chem. **95**, 3358 (1991).
[20] S. W. Rick, S. J. Stuart, and B. J. Berne, J. Chem. Phys. **101**, 6141 (1994).
[21] W. J. Mortier, K. Van Genechten, and J. Gasteiger, J. Am. Chem. Soc. **107**, 829 (1985).
[22] Y. Ma and S. H. Garofalini, J. Chem. Phys. **122**, 094508 (2005).
[23] D. Wolf *et al.*, J. Chem. Phys. **110**, 8254 (1999).
[24] Y. Ma and S. H. Garofalini, Mol. Simul. **31**, 739 (2005).
[25] F. H. Streitz and J. W. Mintmire, Phys. Rev. B **50**, 11996 (1994).
[26] M. Z. Bazant, E. Kaxiras, and J. F. Justo, Phys. Rev. B **56**, 8542 (1997).
[27] J. F. Justo, M. Z. Bazant, E. Kaxiras, V. V. Bulatov, and S. Yip, Phys. Rev. B **58**, 2539 (1998).
[28] A. Aguado and P. A. Madden, Phys. Rev. B **70**, 245103 (2004).
[29] A. A. Maradudin *et al.*, *Theory of Lattice Dynamics in the Harmonic Approximation* (Academic Press, New York, 1971).

[30] M. Striefler and G. Barsch, Phys. Rev. B **12**, 4553 (1975).
[31] M. Born and K. Huang, *Dynamical Theory of Crystal Lattices* (Oxford University Press, London, 1954).
[32] J. R. Ray, Comput. Phys. Rep. **8**, 109 (1988).
[33] J. R. Ray, M. C. Moody, and A. Rahman, Phys. Rev. B **32**, 733 (1985).
[34] S. Nosé, Mol. Phys. **52**, 255 (1984).
[35] W. G. Hoover, Phys. Rev. A **31**, 1695 (1985).
[36] M. Parrinello and A. Rahman, Phys. Rev. Lett. **45**, 1196 (1980).
[37] G. J. Martyna *et al.*, Mol. Phys. **87**, 1117 (1996).
[38] E. Demiralp, T. Cagin, and William A. Goddard III, Phys. Rev. Lett. **82**, 1708 (1999).
[39] B. Dorner, H. Grimm, and H. Rzany, J. Phys. C **13**, 6607 (1980).
[40] J. F. Scott and S. P. S. Porto, Phys. Rev. **161**, 903 (1967).
[41] T. Barron, C. Huang, and A. Pasternak, J. Phys. C **9**, 3925 (1976).
[42] R. G. Della Valle and H. C. Andersen, J. Chem. Phys. **94**, 5056 (1990).
[43] S. H. Garofalini, J. Chem. Phys. **76**, 3189 (1982).
[44] C. T. Kirk, Phys. Rev. B **38**, 1255 (1988).